PHYSICAL REVIEW C VOLUME 57, NUMBER 3 MARCH 1998

Splintering central collisions: Systematics of momentum and energy deposition for (17–115)A MeV ^{40}Ar

E. Colin,[1,4] Rulin Sun,[1] N. N. Ajitanand,[1] John M. Alexander,[1] M. A. Barton,[6] P. A. DeYoung,[6] A. Elmaani,[1,*] C. J. Gelderloos,[7] E. E. Gualtieri,[5] D. Guinet,[4] S. Hannuschke,[5] J. A. Jasma,[6] L. Kowalski,[2] Roy A. Lacey,[1] J. Lauret,[1,3] E. Norbeck,[5] R. Pak,[5] G. F. Peaslee,[6] M. Stern,[4] N. T. B. Stone,[5] S. D. Sundbeck,[6] A. M. Vander Molen,[5] G. D. Westfall,[5] and J. Yee[5]

[1]*Department of Chemistry, State University of New York at Stony Brook, Stony Brook, New York 11794*

[2]*Department of Physics and Geoscience, Montclair State College, Upper Montclair, New Jersey 07043*

[3]*Institut des Sciences Nucléaires de Grenoble, Institut National de Physique Nucléaire et de Physique des Particules-Centre Nationale de la Recherche Scientifique/Université Joseph Fourier, 53 Avenue des Martyrs, 38026, Grenoble Cedex, France*

[4]*Institut de Physique Nucléaire de Lyon, Institut National de Physique des Particules-Centre National de la Recherche Scientifique/ Université Claude Bernard, 43, Boulevard du 11 Novembre 1918, 69622, Villeurbanne Cedex, France*

[5]*National Superconducting Laboratory, Michigan State University, E. Lansing, Michigan 48824*

[6]*Departments of Chemistry and Physics, Hope College, Holland, Michigan 49423*

[7]*Nuclear Physics Laboratory, University of Colorado, Boulder, Colorado 80309-0446*

(Received 6 August 1997)

Measurements are reported for fragment masses and velocities from the reactions (17–115)A MeV ^{40}Ar+Cu, Ag, and Au. Charged particle multiplicities were used to select the most violent reactions, and systematics are reported for the momentum and energy deposition. These reactions are fusionlike for $\lesssim 44A$ MeV ^{40}Ar with a large fraction of momentum and energy deposition in the heavy nuclear system. However, for $\gtrsim 44A$ MeV ^{40}Ar, a majority of the projectile energy and momentum is carried away by a multibody spray of light ejectiles and only a minority is deposited in the heavy nucleus. Nevertheless heavy composite systems are formed with up to 9–12 MeV per source nucleon for 115A MeV ^{40}Ar. [S0556-2813(98)50603-6]

PACS number(s): 25.70.Jj, 25.70.Pq

Near central collisions between heavy ions can lead to very highly excited nuclei whose properties are currently of great interest. For mass asymmetric reactions at only slightly above barrier energies (e.g., $\lesssim 10A$ MeV) there is essentially complete fusion and essentially complete thermalization into a compound nucleus, e.g., [1]. As the incident energy is increased from $\sim 10A$ to $35A$ MeV, the fractional momentum transfer in such fusionlike reactions slowly declines, e.g., [2,3] and is accompanied by a small percentage of forward-peaked, prethermalization particles, e.g., n, ^{1,2,3}H, and ^{4}He. For higher, but still intermediate energies, (e.g., $\sim 35A$ to $150A$ MeV), attention to date has been mainly focused on testing models for multifragmentation of the hot nuclei produced, and a consistent picture has not emerged for the dynamical mechanisms of energy dissipation and thermalization.

One class of experiments (emphasizing very heavy target-projectile pairs) implies an essential domination by two-body, deeply inelastic reactions, even for the central collisions, e.g., [4,5]. Another implies a possible continuation of incomplete fusion, possibly followed by very rapid and even explosive decay into fragment and particle emission, e.g., [5]. This latter process could (and is often assumed to) send out a cloud of small ejectiles and leave no heavy residual nucleus, e.g., [6]. Such a situation is difficult to analyze since measurements of heavy residual nuclei provide the classic probes of linear momentum and energy transfer, e.g., [2,3]. Their associated multiplicities for near isotropic ejectiles also give major probes of the initial energy deposition, e.g., [7]. The combination of such measurements has not been jointly pursued for intermediate energy heavy ion reactions, particularly including the rather slow moving, heavy fragments [8]. In this experiment for (8–115)A MeV (320–4600 MeV) ^{40}Ar+Cu, Ag, Au, we measure mass and velocity of the heavy residual nuclei in conjunction with near 4π detection of light charged particles and fragments [9]. The results lead to an overview of the evolution of incomplete fusion [$\approx$(8–44)A MeV] into splintering central collisions [$\approx$(44–115)A MeV], a new mechanistic classification. Important insights are also given into the interplay between deposition energy and prethermal ejectile spray.

The Michigan State University K1200 cyclotron delivered ^{40}Ar beams from (8–115)A MeV, i.e., from near barrier to well above Fermi energies. The MSU 4π array provided both a multiplicity filter and an overview of angles, energies and identities of charged particles, and fragments [9]. Along with the basic ''soccer-ball'' array from $\sim 18°$ to $\sim 162°$, three forward-angle detection devices were used: (a) the zero degree detector (ZDD), a ring of 8 plastic telescopes covering polar angles of $\sim 0.5°$ to $1.5°$ [10], (b) the Maryland forward array (MFA), a second ring of plastic telescopes from $\sim 1.5°$–$3°$ [11], and (c) a set of 45 Si detectors (~ 2 cm$\times 2$ cm$\times 140$ μm) mounted ≈ 70 cm from the target in front of the 45 telescopes (~ 3 °C to 18°) of the high-rate

*Present address: Battelle Pacific Northwest National Laboratory, National Security Division, Box 999, K6-48, Richland, WA 99352.

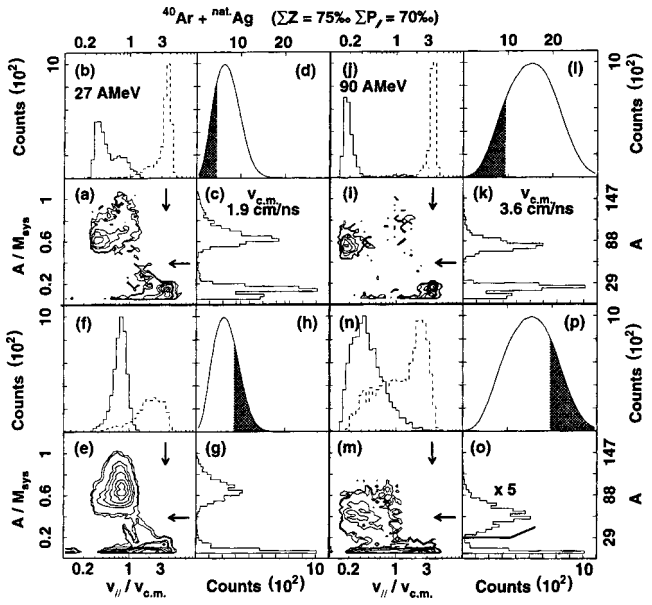

FIG. 1. (a) Contour maps for mass number A vs longitudinal velocity $V_{\parallel}$ of fragments of $A \geq 8$. For uniformity we use dimensionless variables $A/M_{\rm sys}$ and $V_{\parallel}V_{\rm c.m.}$ (log scale). Arrows indicate values for the projectile. (b) Projections from (a) onto the velocity axis with solid line for the heaviest fragment and dashed for all other fragments. (c) Projection onto the mass axis. (d) Overall multiplicity distribution with gate zone shaded. Additional gates on the total detected charge Z were $\geq 75\%$ of $(Z_p + Z_t)$ and on the total detected longitudinal momentum $P_{\parallel}$ were $\geq 70\%$ of the projectile momentum. The quadruplets (e)–(h), (i)–(l), and (m)–(p) are for other multiplicity cuts or incident energies as indicated.

array (HRA) [9]. Bragg-curve ionization chamber ΔE detectors were also used from $\sim 18°$ to 162° in front of each of the 170 telescopes in the ball [9]. Data from the plastic and gas detectors were recorded as described elsewhere, e.g., [12], but only if two or more telescopes fired in the ball. In addition, energy (E) and time of flight (TOF) signals were recorded from each Si wafer. The E and TOF data from these Si detectors were corrected [13] and analyzed to give masses (resolution $\pm 5-10\,\%$) for the slow moving fragments ($A \gtrsim 10$), while data from the other telescopes were analyzed to give atomic numbers and energies for fragments of $Z \sim 1-18$ [9,14].

Figure 1 shows results for heavier fragments from 27A and 90A MeV ^{40}Ar+Ag displayed as functions of longitudinal velocity $V_{\parallel}$ (log scale) and mass number (for $A \geq 8$). Comparison of results from various reaction systems is aided by using the dimensionless variables $V_{\parallel}/V_{\rm c.m.}$ and $A/M_{\rm sys}$, where $V_{\rm c.m.}$ is the c.m. velocity (indicated for each reaction), and $M_{\rm sys} = A_{\rm target} + A_{\rm projectile}$. Figure 1 is divided into four sets of four plots, for example 1(a)–1(d); Figure 1(a) shows a contour map in the plane of $V_{\parallel}/V_{\rm c.m.}$ vs $A/M_{\rm sys}$ while Figs. 1(b) and 1(c) give the projections on each axis. Figure 1(d) shows the overall multiplicity distribution for this reaction with shading to indicate the multiplicity cut used for Figs. 1(a)–1(c). The velocity distributions [Fig. 1(b)] are separated into a solid line for the heaviest fragment in each event and a dashed line for other fragments. Random coincidences with elastically scattered projectiles were eliminated by a software cut on $A \geq 32$ and $V_{\parallel} \geq 0.8 V_{\rm projectile}$. For all the plots shown here we have required that the total detected charge $Z_{\rm obs} \geq 0.75(Z_{\rm target} + Z_{\rm projectile})$ and that the total longitudinal momentum $P_{\parallel} \geq 0.7(P_{\rm projectile})$.

Fragments from 27A MeV ^{40}Ar+Ag are shown in Fig. 1 with a low-multiplicity cut in panels 1(a)–1(d) and with a high-multiplicity cut in panels 1(e)–1(h). First, for the more violent reactions shown in Figs. 1(e)–1(h), we see a dominant peak for the well-known incomplete fusion process with evaporation residue mass $A \sim 90$ and $V_{\parallel}/V_{\rm c.m.} \sim 0.8$ [e.g., 3] In coincidence with these residues are lighter fragments with $A \sim 10$ and $0.3 \lesssim V_{\parallel}/V_{\rm c.m.} \lesssim 4$. These intermediate mass fragments (IMF's) are predominantly forward peaked in either the c.m. or the heavy fragment frame with about one IMF per heavy fragment for this particular case of 27A MeV Ar+Ag [15]. Hence they are not ejected from an equilibrated composite system.

Next we turn to the less violent reactions shown in Fig. 1(a)–1(d) where we see clear signatures of the well-known deep-inelastic reactions (DIR). There is a projectilelike fragment (PLF) with velocity and mass near to that of the projectile ($A \sim 30$, $V_{\parallel}/V_{\rm c.m.} \sim 3.7$) and a targetlike fragment (TLF) with mass near to that of the target ($A \sim 90$) and a very slow speed of $0.25 \lesssim V_{\parallel}/V_{\rm c.m.} \lesssim 0.5$. In addition, there is a small shoulder in Fig. 1(b) for $V_{\parallel}/V_{\rm c.m.} \sim 0.8$ that indicates some remaining heavy nuclei from fusionlike reactions in spite of this low-multiplicity gate.

Turning now to the right-hand panels in Figs. 1(i)–1(p) we can see how the reactions evolve from 27A to 90A MeV. For the low-multiplicity cut [Fig. 1(i)–1(l)] the fast PLF's and slow TLF's (here with $V_{\parallel}/V_{\rm c.m.} \sim 0.18$) are still dominant as is the case for all of the more peripheral reactions for all targets and energies. By contrast for the high-multiplicity cut [Figs. 1(m)–1(p)] we see a heavy fragment with $A \sim 60$ and $V_{\parallel}/V_{\rm c.m.} \sim 0.3$ along with very light IMF's of $A \sim 10$ and a wide range of velocities, $0.2 \lesssim V_{\parallel}/V_{\rm c.m.} \lesssim 4$. It is this class of reactions that we refer to as splintering central collisions. The projectile has been shattered or splintered into a number of light fragments and particles, largely forward peaked in the c.m. frame (Fig. 3 discussed below) and with a wide range of longitudinal velocities. A heavy fragment remains, moving rather slowly ($V_{\parallel}/V_{\rm c.m.} \sim 0.3$), but carrying more than 1/4 of the momentum from the collision. The majority of the momentum is distributed over the set of light ejectiles comprising a forward-peaked spray.

Figure 2 shows the evolution with energy of the violent collision group for ^{40}Ar+Ag. We see that the heaviest fragment group changes with energy in a very regular way. Its average velocity ratio $V_{\parallel}/V_{\rm c.m.}$ drops steadily from ~ 0.9 at 17A MeV, ~ 0.3 at 115A MeV, and similarly its average observed mass number $A_{\rm obs}$ drops from ~ 110 to ~ 55. The linear momentum transfer drops below 50% for incident energies of $\gtrsim 44A$ MeV, and for 65, 90, and 115A MeV the major part of the momentum is carried away by the complex spray of light ejectiles. This behavior is very similar for each target.

As shown in Figs. 1 and 2 the light fragments from the high-multiplicity reactions are really quite different from PLF's. Their average masses are much smaller ($A \sim 10$), and their velocity distributions are much broader. Their average velocity ratios $\langle V_{\parallel}/V_{\rm c.m.} \rangle$ are greater than unity, but they have broad peaks spreading far away from the projectile ve-

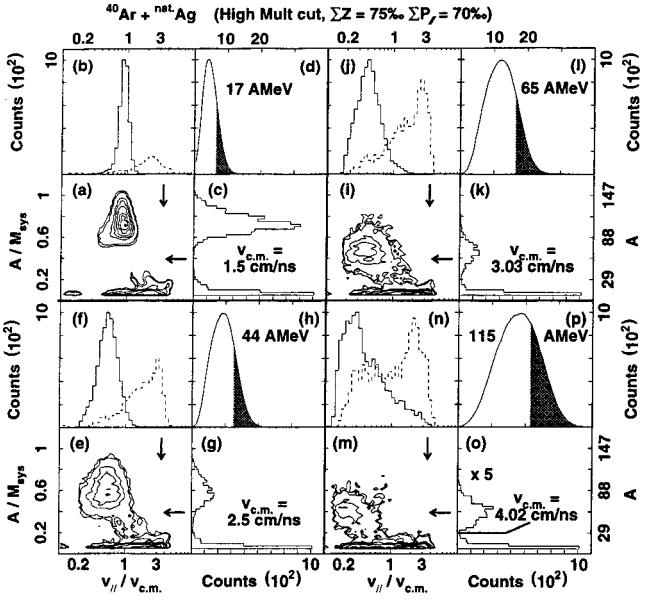

FIG. 2. Same as Fig. 1 for incident energies as indicated.

locities, unlike the PLF's from the more peripheral reactions. Figure 3 addresses the momentum balance and multiplicities for ^{40}Ar+Ag. In panel 3(a) we show the average velocity ratios and in 3(b) the average multiplicities for various ejectiles. In each case (Fig. 3a) the heaviest fragment group ($A>50$) moves more slowly than $V_{\mathrm{c.m.}}$, while all the light fragments and particles have $\langle V_{\parallel}/V_{\mathrm{c.m.}}\rangle \sim 1.5-2$. This angular asymmetry is the hallmark of prethermal ejection, driven by the early reaction dynamics. These lighter ejectiles comprise the spray that carries away an increasing fraction of the momentum with increasing energy. As the incident energy is

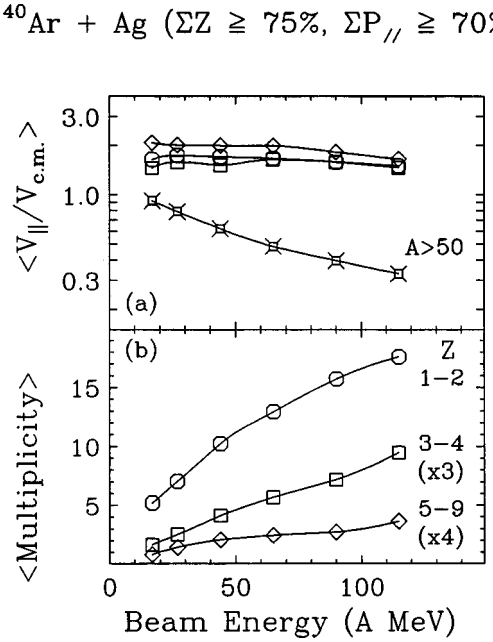

FIG. 3. (a) ^{40}Ar+Ag: Average velocity ratio $\langle V_{\parallel}/V_{\mathrm{c.m.}}\rangle$ for heavy fragments of $A\geq 50$ (i.e., an average over each relevant peak in Fig. 2) and for lighter ejectile groups in correlation with them (averages over 4π sr). (b) Average observed multiplicities of these light fragment groups in coincidence with a fragment of $A\geq 50$.

increased, the multiplicities increase for all the light ejectiles, and correspondingly for the heaviest fragment the value of $\langle V_{\parallel}/V_{\mathrm{c.m.}}\rangle$ decreases steadily. Roughly speaking the light ejectiles comprise only $\sim$10% of the total mass for 17A MeV (e.g., see Table I in Ref. [3]), while they increase to $\sim$50% for 115A MeV. Correspondingly the mass of the typical observed heavy fragment decreases from $\sim$90% to $\lesssim$50% of the total mass.

It is this complex of light ejectiles with $\langle V_{\parallel}/V_{\mathrm{c.m.}}\rangle \geq 1$, mainly attributable to the spalled projectile, that carries away most of projectile's linear momentum in the central collisions (for $\gtrsim$65A MeV). The patterns in Figs. 2 and 3 demonstrate a continuous evolution for these most violent collisions from essentially complete fusion or $\langle V_{\parallel}/V_{\mathrm{c.m.}}\rangle \sim 1$ at 8A MeV (not shown) to more incomplete fusion at 27A and 44A MeV and then to splintering central collisions for 65A to 115A MeV. There is no dramatic signal designating an exit from the ''fusion compound nucleus domain'' or an entry into the ''Fermi energy domain.'' However, there is a strong and definite evolution observed in the velocity ratios for the heavy residual nuclei [Fig. 3(a)] that changes over from majority momentum acceptance to minority momentum acceptance, at $\sim$44A MeV. The projectile seems to have been shattered in the reaction zone into nucleons and other light fragments whose velocities are degraded and spread out as they traverse the target and assault the mean field barrier to their escape. Some of the splinterlike ejectiles of these shattered projectiles successfully penetrate through the barrier, and we see them in one of the detector arrays. Certain others are captured into a composite nuclear system, which is collisionally driven toward thermalization. Over the span of 8A to 115A MeV for these ^{40}Ar+Ag reactions, the fraction of transferred momentum decreases from $\sim$100% to $\sim$30% (Fig. 3), and the multiplicity of the forward peaked light ejectiles strongly increases.

In Fig. 4(a) we summarize for all targets the pattern of average observed masses and velocities for the heaviest fragments from the more violent collisions. The average mass number of the light fragments is $\sim$ 10 for all reactions (high-multiplicity cut). The average mass observed for the heavy fragment group, decreases monotonically with incident energy for each target as does the average velocity ratio $\langle V_{\parallel}/V_{\mathrm{c.m.}}\rangle$ as shown in Fig. 4(b). The behavior is very similar for Cu, Ag, and Au targets.

From the values shown in Fig. 4 we have estimated the average momentum and excitation energy deposited into the heavy composite nuclei. For simplicity we use the straightforward one-dimensional approximation; one assumes that a fraction f of the projectile mass A_p, charge Z_p, and momentum fuses with the target of Z_tA_t into a composite nuclear system of Z_cA_c:

$$(fZ_p, fA_p)+(Z_t, A_t)\rightarrow(Z_c, A_c)+Q_f \quad \text{and} \quad A_c=fA_p+A_t.$$

Then one has

$$V_p(fA_p)=V_{\parallel}(A_c) \quad \text{and} \quad E^*=fE_p[A_t/(A_t+fA_p)]+Q_f$$

in contrast to the case for complete fusion, where

$$V_p(A_p)=V_{\mathrm{c.m.}}(A_t+A_p) \quad \text{and} \quad E^*=E_{\mathrm{c.m.}}+Q.$$

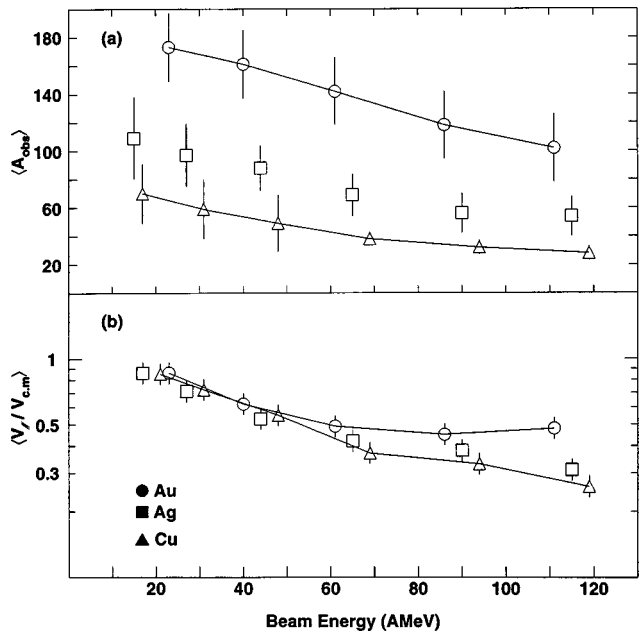

FIG. 4. ^{40}Ar+Cu, Ag, Au: (a) Average mass number $\langle A\rangle_{\rm obs}$ for the heaviest observed fragments for the high-multiplicity cut (highest 15%) with gates as shown in Figs. 2 and 3. Bars show the full width at half maximum. (b) Average velocity ratios $\langle V_{\|}V_{\rm c.m.}\rangle$ for the same fragment group. For clarity triangles for Cu (circles for Au) are displaced horizontally by $+4A$ $(-4)A$ MeV. Bars show statistical uncertainties.

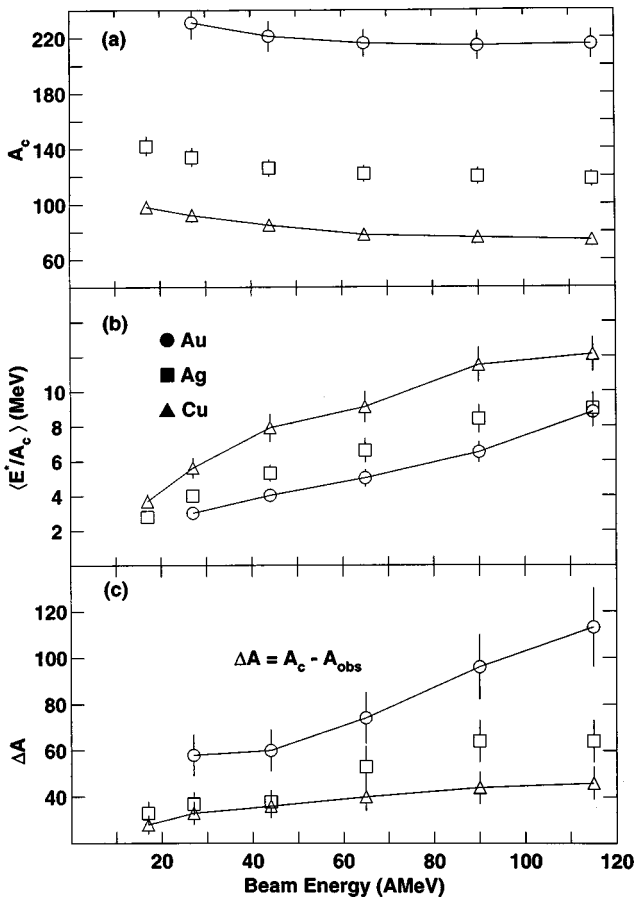

FIG. 5. (a) Average mass number of the initial heavy composite nucleus. (See text.) (b) Average initial excitation energy per nucleon in the groups of heavy composite nuclei. (c) Average mass ejected from the initial heavy composite nuclei, ΔA.

We measure $V_{\|}/V_{\rm c.m.}$ and thus can obtain f, A_c, and E^* for each heavy reaction system. This initial heavy composite system is then assumed to emit fragments and particles nearly isotropically giving a final observed system with mass number $A_{\rm obs}$ as reported in Fig. 4(a).

These estimates of the masses and reaction energetics are summarized in Fig. 5. The average initial masses A_c of the heavy composite nuclei are shown in Fig. 5(a); they vary rather slowly with energy. The excitation energy per source nucleon E^*/A_c is shown in Fig. 5(b); it increases regularly with incident energy. The average mass ejected by these hot nuclei can be obtained from the difference $\Delta A=A_c-A_{\rm obs}$ and is shown in Fig. 5(c). It increases with target mass and incident energy following the initial excitation E^*.

For 17A MeV ^{40}Ar one obtains heavy nuclei excited to $\sim$2–3 MeV/nucleon; this excitation increases to 9–12 MeV/nucleon for 115A MeV [Fig. 5(b)]. The initial composite system mass decreases with energy also, but by a relatively small amount [Fig. 5(a)]. These central collisions can be said to change gradually from incomplete fusion (IF) with capture of most of the projectile [e.g., 3] to splintering central collisions (SCC) with capture of only a minority fraction of the projectile nucleons. The early reaction dynamics generate a multibody spray of nucleons and fragments ejected in the forward direction (i.e., that of the Ar projectile). One might say that the relationship of SCC to IF for the early reaction history is analagous to the relationship of statistical multifragmentation to statistical evaporation for the late reaction history.

To summarize this study of $(8-115)A$ MeV ^{40}Ar+Cu, Ag, Au, we have presented measurements of near 4π detection of light charged ejectiles along with slow moving heavier nuclei. These heavy fragments provide an invaluable probe for the momentum balance. For $(8-44)A$ MeV the results for the most violent collisions show majority momentum transfer typical of complete and incomplete fusion. For $(65-115)A$ MeV the most violent reactions exhibit majority momentum retention by a multibody ejectile spray from splintering central collisions. This spray consists of a complex collection of light charged ejectiles, forward peaked, but with a wide range of velocities that is very different from the incident projectile. Analyses and models of multifragment emission must address these prethermal ejectiles. By using the central collision group as described above, one can produce heavy composite nuclei with large and systematic changes in their excitation energy, but rather limited changes in their average initial mass. This can be of great utility in the search for nuclear liquid-gas phase changes, currently a very controversial topic [16].

[1] R. Bass, *Nuclear Reactions with Heavy Ions* (Springer-Verlag, New York, 1980).
[2] H. Morgenstern, *et al.*, Phys. Rev. Lett. **52**, 1104 (1984); V. E. Viola *et al.* Nucl. Phys. **A502**, 531c (1989); F. Haddad *et al.* Phys. Rev. C **53**, 1437 (1996).
[3] M. T. Magda *et al.*, Phys. Rev. C **53**, R1473 (1996).
[4] B. M. Quednau *et al.*, Phys. Lett. B **309**, 10 (1993).
[5] *Nuclear Chemistry Award Symposium honoring Joseph B. Natowitz*, American Chemical Society, Anaheim, California, 1995 (World Scientific, Singapore, 1997).
[6] G. Auger *et al.*, Phys. Lett. **169B**, 161 (1986).
[7] E. Piasecki *et al.*, Phys. Rev. Lett. **66**, 1291 (1991).
[8] A. Yokoyama *et al.*, Phys. Rev. C **46**, 647 (1992).
[9] G. D. Westfall *et al.*, Nucl. Instrum. Methods Phys. Res. A **238**, 347 (1985); M. Maier *et al.*, *ibid.* **337**, 619 (1994); A. M. Vander Molen *et al.*, Trans. Nucl. Sci. **41**, 80 (1984); R. Pak Ph.D. thesis, Department of Physics, Michigan State University, 1996.
[10] N. T. B. Stone, Ph.D. thesis, Department of Physics, Michigan State University, 1996.
[11] N. D. Russ, Ph.D thesis, University of Maryland, 1996.
[12] W. J. Llope *et al.*, Phys. Rev. C **52**, 1900 (1995).
[13] J. B. Moulton *et al.*, Nucl. Instrum. Methods Phys. Res. A **157**, 325 (1978).
[14] D. A. Cebra *et al.*, Nucl. Instrum. Methods Phys. Res. A **300**, 518 (1991).
[15] D. Jouan *et al.*, Z. Phys. A **340**, 63 (1991).
[16] See, e.g., J. B. Natowitz *et al.*, Phys. Rev. C **52**, R2322 (1995).